

Ferroelastic phase transition in $\text{Cs}_3\text{Bi}_2\text{I}_9$: A neutron diffraction study

A. Jorio*

Departamento de Física, Universidade Federal de Minas Gerais, Caixa Postal 702, 30123-970, Belo Horizonte, Minas Gerais, Brazil

R. Currat, D. A. A. Myles, and G. J. McIntyre

Institut Laue-Langevin, Boîte Postale 156, 38042 Grenoble Cedex 9, France

I. P. Aleksandrova

L.V. Kirensky Institute of Physics, Krasnoyarsk, 660036, Russia

J. M. Kiat

*LSPMM (UMR CNRS NR 8580), Ecole Centrale Paris, Chatenay-Malabry cedex, France
and LLB, CEN Saclay, 91191 Gif-sur-Yvette cedex, France*

P. Saint-Grégoire

Université de Toulon et du Var, LMMI, Boîte Postale 132, 83957 La Garde cedex, France

(Received 27 September 1999)

Crystalline $\text{Cs}_3\text{Bi}_2\text{I}_9$, with the $P6_3/mmc$ symmetry at room temperature was studied by Laue and four-circle neutron diffractometry from room temperature down to 50 K. At $T_0=220$ K the crystal undergoes a second-order proper ferroelastic phase transition to a polydomain structure with a nonprimitive monoclinic $C12/m1$ space group. Satellites were not found below T_0 , indicating that the continuous distribution of sites observed in previous ^{127}I nuclear quadrupole resonance experiments is due either to an undetected incommensurate phase characterized by a very small displacement amplitude, or due to the fraction of the crystal volume occupied by domain walls. We argue that thick domain walls are expected in the present structure due to the absence of mechanical compatibility between domains.

I. INTRODUCTION

The $A_3B_2X_9$ family has been studied extensively during the last few decades and has revealed a variety of different structural phases and phase transitions.¹⁻⁵ Recently, several publications have appeared on compounds in this family, showing interesting effects including the possible appearance of incommensurate phases as in the $\text{Cs}_3\text{Bi}_2\text{I}_9$ compound which is the subject of this work.

At room temperature (phase I) $\text{Cs}_3\text{Bi}_2\text{I}_9$ exhibits a $P6_3/mmc(D_{6h}^4, \text{No. } 194)(Z=2)$ structure, with lattice parameters $a=8.404$ Å and $c=21.183$ Å (Ref. 1) (see Fig. 1). Melnikova *et al.*⁵ studied the temperature evolution of the birefringence, dielectric and elastic constants, and performed differential scanning calorimetry (DSC) and nuclear quadrupole resonance (NQR) experiments. At $T_0=220$ K there occurs a transition to a phase labeled II, characterized by the nearly complete softening of the C_{44} elastic constant, and accompanied by the appearance of birefringence for light propagating along the $[001]$ direction (Δn_c), and by the splitting of the NQR ^{127}I lines into triplets and doublets below T_0 . These results led to the conclusion that there exists in $\text{Cs}_3\text{Bi}_2\text{I}_9$ a proper ferroelastic second-order phase transition with a symmetry change from the hexagonal $6/mmm$ to the monoclinic $2/m$ point group. X-ray results obtained by Aleksandrova *et al.*⁶ are in agreement with the reported $P6_3/mmc$ structure determination¹ for phase I and a symmetry reduction to $2/m$ in phase II with $P12_1/m1$ as the suggested space group, and lattice parameters a

$=8.508$ Å, $b=14.380$ Å, $c=21.095$ Å, $\beta=90.608^\circ$.

However, the most interesting result is given by NQR measurements:^{6,7} the shape of the split lines below $T_0=220$ K indicates the presence of a continuous distribution of sites as typically observed in incommensurate phases. We emphasize that the presence of a lock-in phase transition was not detected. Moreover, the number of NQR ^{127}I lines below the transition point and the character of the observed splittings are in agreement with a transition that takes place near the center of the Brillouin zone. In such a case, there is no Lifshitz term in the thermodynamic potential, and the existence of an incommensurate phase leads to the question of identifying the mechanism responsible for it. On the other hand, the temperature dependence of C_{44} (which softens nearly to zero at the transition point) confirms that the instability occurs at or in the close vicinity of the Brillouin-zone center. The size of the primitive unit cell (or average primitive unit cell in the case of a modulated structure^{6,7}) is thus expected to be the same in phase I as in phase II.

In this work we performed a careful neutron-diffraction study to understand better the nature of the phase transition and to answer some of the remaining open questions, in particular that concerning the possible existence of an intermediate incommensurate phase just below T_0 . Neutron diffraction was chosen to ensure that we observe the behavior of the bulk of the sample.

II. EXPERIMENT

$\text{Cs}_3\text{Bi}_2\text{I}_9$ single crystal (0.5 cm^3) was grown by the Bridgman method in argon-filled quartz ampoula with CsI

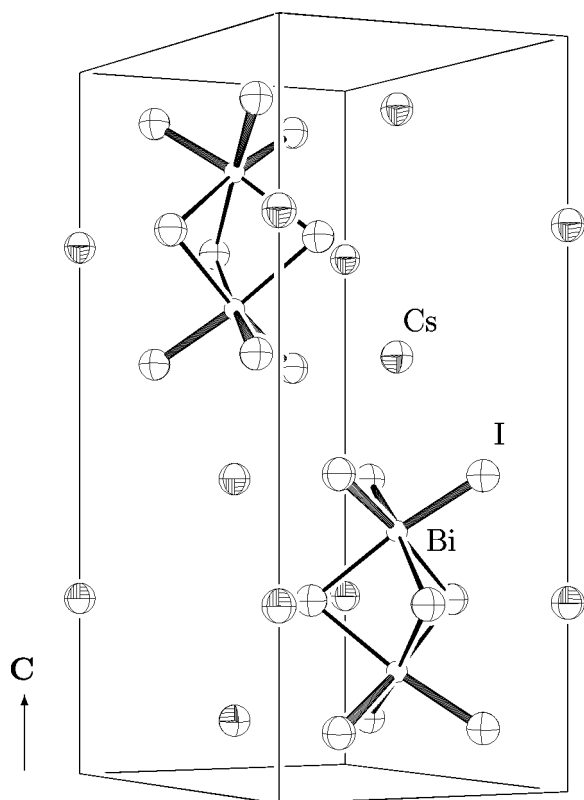


FIG. 1. The $\text{Cs}_3\text{Bi}_2\text{I}_9$ unit cell at room temperature (atomic positions from Ref. 1).

and SbI_3 taken in stoichiometric proportion. $\text{Cs}_3\text{Bi}_2\text{I}_9$ was studied by means of neutron diffraction at the Institut Laue-Langevin using Laue and four-circle diffractometers.

A. Laue diffraction

Laue diffraction experiments were performed on LADI, an instrument installed on a cold neutron guide end station. A wavelength band centered at 3.5 \AA and with $d\lambda/\lambda = 25\%$ was used. The beam was collimated to match the sample size using a 2.2-mm LiF circular aperture. The instrument LADI uses a large neutron sensitive image-plate detector, mounted on a cylindrical camera (radius 159.2 mm and length 400 mm) that almost completely surrounds the sample.⁸ The sample was mounted on a small goniometer head attached to the cold tip of an Edwards closed cycle refrigerator. The sample could be rotated around the common axis of the refrigerator and the cylindrical detector.

In Laue diffraction, the crystal is irradiated with a neutron beam which is broad and continuous in wavelength. This provides an extensive survey of the reciprocal space of the illuminated sample. Laue diffraction was performed at different temperatures for several crystal orientations. Several Laue pictures were obtained with the crystal mounted with its hexagonal c -axis first perpendicular and then parallel to the cylinder rotation axis; exposures were made for several rotation angles, giving sufficient information about the reciprocal lattice. The experiment was performed at several temperatures from 60 K up to room temperature, with particular attention in the region below $T_0 = 220 \text{ K}$, identified as the potential incommensurate transition temperature.^{6,7} Long

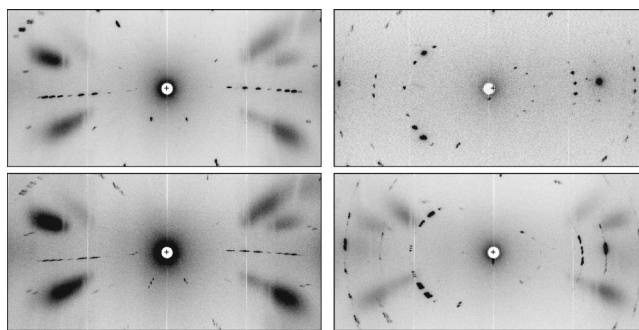


FIG. 2. Neutron Laue diffraction pattern of $\text{Cs}_3\text{Bi}_2\text{I}_9$ with the hexagonal c axis of the crystal parallel (left-hand-side pictures) and perpendicular (right-hand-side pictures) to the incident beam direction, at room temperature (upper pictures) and at 60 K (lower pictures).

time exposures (60–600 min) were used in order to detect any indication of weak reflections. No such superlattice reflections were observed.

B. Monochromatic four-circle diffraction

For detailed examination of individual reflections the four-circle diffractometer $D10$, installed on a thermal-neutron guide was used operating at a wavelength of 2.36 \AA from a pyrolytic graphite (0 0 2) monochromator chosen as a compromise between intensity and momentum resolution. The sample was mounted in a helium-flow cryostat,⁹ which allows full four-circle angular access in the temperature range from 1.6 to 300 K. The temperature behavior of the (006), $(4\bar{2}0)$, (400), (40X), $(X\bar{X}0)$ and $(X00)$, with $X = 1, 2, 3, 4$, $(4\bar{2}2)$, $(4\bar{3}1)$, $(2\bar{1}0)$, $(3\bar{1}0)$, $(3\bar{2}0)$, (224) Bragg reflections was followed between 50 K and room temperature. For the first four reflections, scans were performed in the h, k , and l directions, whereas only the l direction was scanned for the following others. Below the phase transition, various reciprocal space scans were performed through each of the above reflections in order to measure the magnitude of the ferroelastic distortion and to get information on the domain structure. The possibility of incommensurate satellites appearing near Bragg reflections was also investigated. $D10$ is well suited for this type of work due to its good momentum resolution at relatively high flux and low intrinsic background (for more details of LADI and $D10$ see <http://www.ILL.fr/Yellowbook/>).

III. RESULTS AND DISCUSSIONS

A. Laue diffraction

Figure 2 shows four Laue pictures of $\text{Cs}_3\text{Bi}_2\text{I}_9$ obtained with two different crystal orientations, namely with the hexagonal c -axis parallel (left-hand-side frames) and perpendicular (right-hand-side frames) to the neutron incidence direction, at room temperature (upper frames) and at 60 K (lower frames). The broad diffuse streaks present in all pictures are due to the cryostat aluminum walls.

In phase I, the complete set of observed reflections could be indexed using the hexagonal structure lattice parameters, yielding $a = 8.41(1)$ and $c = 21.18(1) \text{ \AA}$. We note here for a better understanding of the results that, at room temperature, some Bragg reflections present several components instead

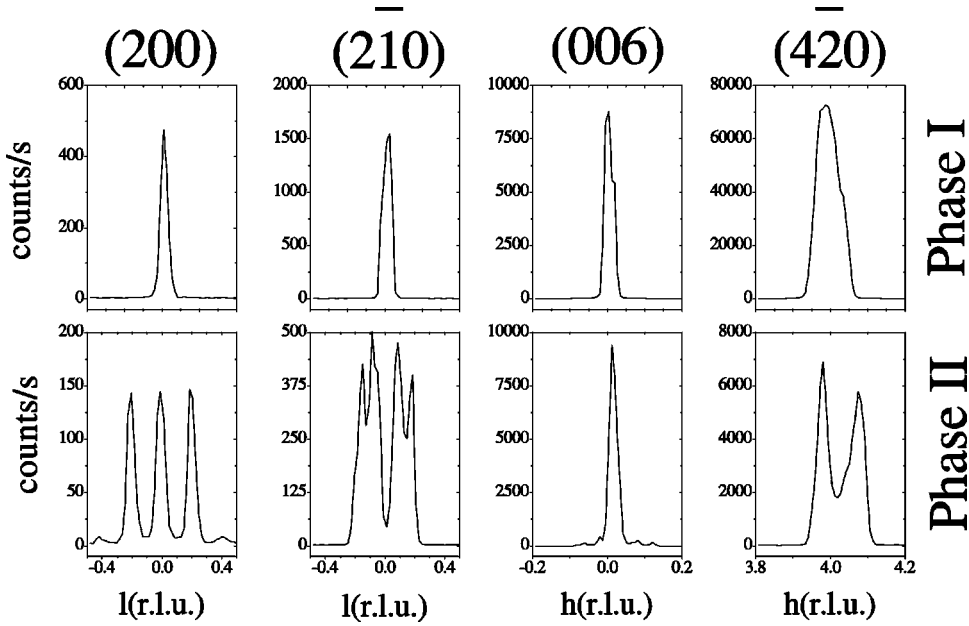


FIG. 3. Four Bragg reflections of $\text{Cs}_3\text{Bi}_2\text{I}_9$ in the room temperature (I) and low-temperature (II) phases. Scans in phase I were performed at $T=230$ K. In phase II, the $(20l)$ and $(h06)$ scans were performed at $T=50$ K, the $(2\bar{1}l)$ scan at $T=100$ K, and the $(4\bar{2}l)$ scan at 60 K.

of a single peak due to an inhomogeneous mosaic structure (see upper pictures in Fig. 2).

The phase transition is characterized by a splitting of most Bragg reflections (see the lower pictures in Fig. 2), due to the ferroelastic nature of the phase transition. The splitting starts at T_0 and exhibits a temperature evolution that will be discussed later. No evidence of doubling of the lattice constant was observed in these images. Long exposure times (600 minutes at $T=60$ K, lower pictures in Fig. 2) revealed no extra diffraction spots, which allows us to discard the primitive $P12_1/m1$ space group with doubling of the unit cell.⁶ This result indicates that the low-temperature phase II occurs via a Brillouin-zone center instability, and the low-temperature Laue pattern can be completely explained by a polydomain structure with a nonprimitive $C12/m1$ (C_{2h}^3 , No. 12) space group. At $T=60$ K the domain structure is clearly resolved, and it is possible to index all diffraction spots by applying sixfold rotations around the hexagonal axis to the spots belonging to a monodomain of $C12/m1$ symmetry. The conclusion that the space group is $C12/m1$ was checked by means of x-ray powder diffraction and the spectrum can indeed be fitted unambiguously within this group; lattice parameters are in good agreement with the neutron results.

Details of the complex diffraction pattern associated with the polydomain structure and ferroelastic deformations below T_0 were investigated by four-circle diffractometry and are analyzed in the next section.

B. Monochromatic four-circle diffraction study

As shown in Fig. 3, below the phase transition at $T_0=220$ K, the ferroelastic deformation causes a splitting of most Bragg reflections into three, four, or more components. There are also some hexagonal reflections that do not split at all. As already pointed out, some Bragg reflections already exhibit more than one component in phase I because of the presence of a grain structure in the sample. We now analyze the splitting pattern which develops below T_0 in terms of the formation of ferroelastic domains.

At the hexagonal-monoclinic phase transition, the order of the point group is reduced from 24 at high temperature to 4 for the subgroup at lower temperature. Consequently the transition gives rise to six single orientational domain states in the monoclinic phase, which can be distinguished by their ferroelastic deformation. The deformation with respect to the parent hexagonal structure is given by the loss of the perpendicularity between the a and c hexagonal axes and by an orthorhombic distortion in the basal plane.

Let us discuss first the loss of the perpendicularity between the a and c hexagonal axes. Considering only this distortion, two orientations of the corresponding domain walls satisfying the condition of mechanical compatibility are possible. However, these two configurations are not energetically equivalent since they are not related by symmetry operations. They are shown in Fig. 4. All the observed Bragg reflections in the hexagonal a^*b^* -plane exhibit a splitting in the c^* direction below the phase transition. The complete profile of these split spots can be explained by a splitting of the a^* axis in the monoclinic phase, which means that the c axis is reoriented, and that the domain walls present would be perpendicular to it [see Fig. 4(I)]. Consider for instance the (200) hexagonal reflection. In the monoclinic phase this reciprocal-lattice position is formed by different reflections from the six different domains, namely $(040), (0\bar{4}0)$,

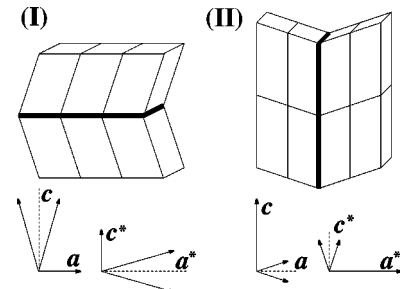


FIG. 4. Two possible domain-wall orientations (bold lines) satisfying the condition of mechanical compatibility for the monoclinic distortion in the low-temperature phase of $\text{Cs}_3\text{Bi}_2\text{I}_9$.

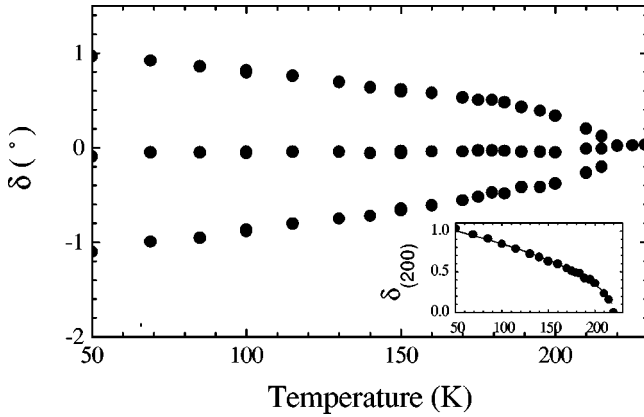


FIG. 5. Splitting of the (200) Bragg reflection of $\text{Cs}_3\text{Bi}_2\text{I}_9$ along the c^* direction. The inset shows the temperature evolution of $\delta_M = \frac{1}{2}[|\delta^+| + |\delta^-|]$ (dots), where δ^+ and δ^- are the splitting of the curves along the $+c^*$ and $-c^*$ directions, respectively. The line is the result of the fit, according to the law $\delta_M = 0.08(220 - T)^{0.5}$.

$(2\bar{2}0)$, $(\bar{2}20)$, (220) , and $(\bar{2}\bar{2}0)$. Since only the a^* axis exhibits a deformation the (040) and the $(0\bar{4}0)$ are unshifted, and the $(2\bar{2}0)$, $(\bar{2}20)$, (220) , and $(\bar{2}\bar{2}0)$ reflections exhibit a shift along $+c^*$ and $-c^*$ direction, depending on the sign of the index h . Therefore, the hexagonal (200) Bragg reflection exhibits a splitting into three components (see Fig. 3). Looking now at the $(2\bar{1}0)$ hexagonal reflection, in the monoclinic phase this reciprocal-lattice position is formed by the $(1\bar{3}0)$, $(\bar{1}30)$, (200) , $(\bar{2}00)$, (130) , and $(\bar{1}\bar{3}0)$ reflections. All these reflections have a component in the a^* direction, consequently, there is no unshifted peak. In the monoclinic phase there are four peaks, two shifted by $\pm\delta$, namely the $(1\bar{3}0)$, $(\bar{1}30)$, (130) , and $(\bar{1}\bar{3}0)$ reflections, and two shifted by $\pm 2\delta$, (200) , and $(\bar{2}00)$. The peaks that are shifted by $\pm\delta$ are more intense than the other two, probably mainly because there are four domain states that have a reflection in the corresponding direction (see Fig. 3) (nevertheless, note that the structure factors of the different monoclinic peaks that cluster near the hexagonal peak may be different, i.e., $|F_{1\bar{3}0}|^2 \neq |F_{130}|^2 \neq |F_{210}|^2$). In the same way we can explain the splitting profile of the other observed reflections. Moreover, the observed $(00X)$ hexagonal reflections ($X=4$ and 6) do not split (see Fig. 3), showing that domain walls perpendicular to the a axis [Fig. 4(II)] do not exist, or may be present only in a very small amount.

Figure 5 shows the temperature evolution of the splitting δ of the (200)-hexagonal reflection along the c^* direction, in degrees. The inset in Fig. 5 shows $\delta_M = \frac{1}{2}[|\delta^+| + |\delta^-|]$ (dots), where δ^+ and δ^- are the splittings along the $+c^*$ and $-c^*$ directions, respectively. This curve could be fitted with the function $\delta_M = A(T_c - T)^{\bar{\beta}}$, with $T_c = 220$ K, $A = 0.08^\circ \text{K}^{-1}$ and the classical $\bar{\beta} = 0.5$ mean-field value. The monoclinic angle β (not to be confused with the exponent $\bar{\beta}$ of the order parameter) can be obtained from the relation $\beta = 90^\circ + \delta$ which yields the value $\beta = 90.67^\circ$ for $T = 143$ K, in agreement with the value reported in Ref. 6. These results are consistent with a transition of the proper ferroelastic type.

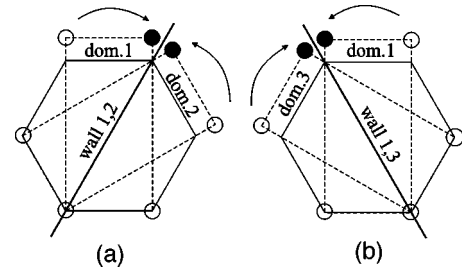


FIG. 6. Schematic representations of the orthorhombic distortions with two possible domain walls parallel to the c axis, satisfying the condition of mechanical compatibility.

The observed splittings along the c^* direction can be completely explained by the monoclinic reorientation of the c axis. However, a splitting of some spots along the a^* and b^* directions was also observed [see, e.g., $(4\bar{2}0)$ in Fig. 3]. This result is related to the orthorhombic distortion in the basal plane. Such a distortion generates three single domain states. A domain wall satisfying the condition of mechanical compatibility should contain the c axis and the common diagonal of the two adjacent orthorhombic domains (see Fig. 6). Note that the formation of this kind of domain wall must be accompanied by a reorientation of the domains: looking at Fig. 6(a), the orthorhombic distortions in the single domain states 1 and 2 are represented by the displacement of the circles out of the hexagonal positions. However, at the domain wall, the two full circles (representing the same object) must naturally coincide, and the two domains will suffer a reorientation as indicated by the arrows (clockwise for domain 1). Looking now at Fig. 6(b), the mechanical compatibility between domain 1 and domain 3 asks for a new reorientation of the domains walls (counterclockwise for domain 1). Nonrotated domains are able to exist only as isolated domains, and in general six different rotated domain states are expected.¹⁰ Hence a simple hexagonal-orthorhombic deformation leads to the formation of six orthorhombic domain states, where the relation $b = \sqrt{3}a$ is no longer satisfied, and the domains are reorientated in order to comply with the condition of mechanical compatibility for the domain walls. The presence of these distortions in the basal plane is evidenced in $\text{Cs}_3\text{Bi}_2\text{I}_9$ by the splitting of some Bragg reflections along the a^* and b^* directions [see, e.g., $(4\bar{2}0)$ in Fig. 3].

We have discussed above the formation of domains and domain walls DW's due first to the monoclinic reorientation of the c axis, and then associated with the orthorhombic distortion in the basal plane, to show in these simple cases what is the domain-wall orientation satisfying mechanical compatibility. However, in $\text{Cs}_3\text{Bi}_2\text{I}_9$ it is clear that the two distortions are simultaneously present. Janovec and Richterová¹⁶ have analyzed ferroelastic domain structures and deduced orientations of domain walls satisfying the condition of mechanical compatibility. It appears that in our case two orientations of a single wall comply with this condition. In a multidomain structure parallel domain walls still comply with it but the situation is completely different if there exist nonparallel DW's in the system because a frustration occurs and DW's can no more satisfy the condition. As a consequence it occurs that all the possible domain-wall orientations cost a large elastic energy, and consequently the domain walls

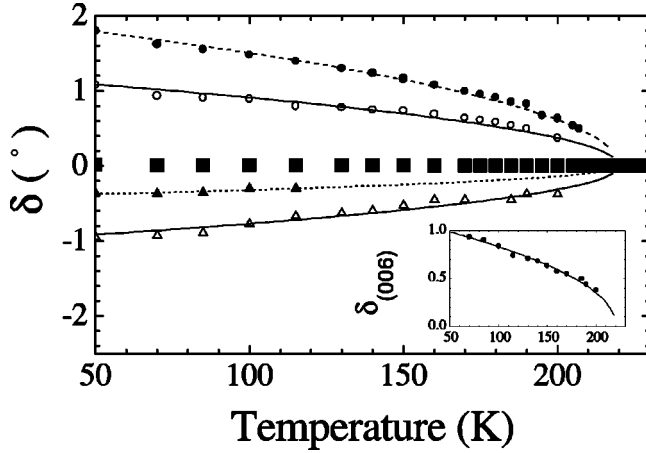


FIG. 7. Temperature evolution of the $(h06)$ scans in Cs₃Bi₂I₉. The large squares refer to the (006) Bragg position. The small circles and triangles show the evolution of the small peaks that appear below T_0 . The lines correspond to fits with the classical law $\delta_M = A(220 - T)^{0.5}$. In the inset the temperature evolution of $\delta_{M'} = \frac{1}{2}[|\delta_{\circ}| + |\delta_{\Delta}|]$ (dots) is shown; δ_{\circ} and δ_{Δ} are the splitting of the small peaks indicated by open circles and open triangles, respectively, and the line represents the fit with the classical law $\delta_M = 0.08(220 - T)^{0.5}$.

should be thick in order to expand the region where the gradient of the order parameter $\nabla \eta$ is nonzero and to minimize the energy cost [proportional to $(\nabla \eta)^2$].

Now that the profile of split peaks is explained, we must still take into account the appearance of small peaks close to some Bragg reflections, below T_0 [see, for example, the small peaks in the $(20l)$ and $(h06)$ scans, shown in Fig. 3]. Although these small peaks may appear as serious candidates as possible incommensurate satellites, the temperature variation of their intensity and position does not follow the standard pattern. In structures with long period incommensurate modulations such as quartz,¹³ NaNO₂,¹⁴ or Sn₂P₂Se₆,¹⁵ satellite peaks grow in intensity on cooling at the same time as they move closer to the parent Bragg reflection, leading to an eventual low temperature lock-in transition. The small peaks seen in Fig. 3 show a very different behavior: their intensity decreases and their separation from the parent Bragg peak increases on cooling (see Fig. 7). Several authors (Loginov¹¹ and Felix *et al.*¹²) have reported a class of incommensurate phases where the wave vector associated with the incommensurate structure increases on cooling, starting from the value 0 at T_l . Phase transitions belonging to this class can occur in systems whose symmetry allows a gradient-cubic term in the free-energy density while forbidding cubic and Lifshitz terms. For an incommensurate phase that takes place in the Brillouin-zone center between two groups that contain the inversion symmetry operation, there is no linear gradient term like $\eta \nabla \eta^*$ and no third-order term like $\eta \eta^* \nabla \eta^*$ since η is even and ∇ is odd with respect to inversion. So, on the basis of symmetry considerations, the occurrence of such an incommensurate phase can be ruled out here.

The appearance of the small peaks is most probably related to the ferroelastic distortion. In fact, the curves shown in Fig. 7 can be very well fitted with the classical law $\delta = A(220 - T)^{0.5}$ (lines in Fig. 7). The inset in Fig. 7 shows $\delta_{M'} = \frac{1}{2}[|\delta_{\circ}| + |\delta_{\Delta}|]$ (dots), where δ_{\circ} and δ_{Δ} are the split-

ting of the small peaks indicated in Fig. 7 by open circles and open triangles, respectively. The fit of this curve gives the same $\tilde{\beta} = 0.5$ and the same $A = 0.08^\circ/\text{K}$ deformation constant obtained for the (200) splitting (see Fig. 5). This result shows that the kind of domain wall depicted in Fig. 4(II) is also present in the crystal in the low-temperature phase, but in a very small amount. Furthermore, the observed decrease of the small peaks intensity below T_0 indicates that the number of this kind of domain walls decreases on cooling.

IV. CONCLUSION

Cs₃Bi₂I₉ exhibits a $P6_3/mmc$ structure at room temperature. At $T_0 = 220$ K the crystal undergoes a ferroelastic phase transition characterized by the splitting of most Bragg reflections. The complete low-temperature diffraction pattern can be indexed assuming a polydomain structure with a non-primitive monoclinic $C12/m1$ unit cell. The major splittings observed show that the low-temperature structure is formed by domains characterized by the reorientation of the c axis along the six equivalent a -axis-type directions, and by a distortion in the basal plane. The classical $\tilde{\beta} = 0.5$ mean-field value found for the temperature evolution of the splittings is in agreement with the assumption of a proper ferroelastic transition. The observation of smaller peaks below T_0 indicates that domains characterized by the reorientation of the a axis are also present, but in a much smaller amount.

Satellites were not found at any low temperature below $T_0 = 220$ K. However, the shape of the split ¹²⁷I NQR lines^{6,7} below T_0 indicates the presence of a continuous distribution of sites typical of incommensurate modulated phases. There are two possible explanations to make these two results compatible: the incommensurate phase may be characterized by a very small amplitude of the atomic displacements, which leaves open questions like why a lock-in phase transition is not observed at low temperatures. It was shown that in the low-temperature phase of Cs₃Bi₂I₉ there is a large number of possible domain states, and that it is not possible to find domain-wall orientations satisfying the condition of mechanical compatibility. In this case, all domain-wall orientations cost a large elastic energy, and the domain walls should be thick. It is reasonable to suppose that the distribution of sites exhibited by the ¹²⁷I lines in the NQR experiments^{6,7} is due to the part of the crystal volume lying within the domain walls, which is expected to include a large distribution of different sites. This argument should apply to all ferroelastics with a large number of domain states, in which the condition of mechanical compatibility cannot be fulfilled. Their resonance spectra should be characterized by a distribution of sites resembling that of an incommensurate structure. This point will be checked in further studies.

ACKNOWLEDGMENTS

We would like to acknowledge the assistance of M. A. Pimenta and N. L. Speziali for a critical reading of the manuscript. One of us (A.J.) is grateful to the Agencies CAPES and CNPq for financial support. The work is partially supported by Grant No. INTAS 97-0177.

*Electronic address: adojoorio@fisica.ufmg.br

- ¹B. Chabot and E. Parthé, *Acta Crystallogr., Sect. B: Struct. Crystallogr. Cryst. Chem.* **34**, 645 (1978).
- ²I.P. Aleksandrova, A.A. Sukhovskii, S.V. Mel'nikova, L. I. Shabanova, and A. I. Zaitsev, *Fiz. Tverd. Tela (St. Petersburg)* **39**, 946 (1997) [*Phys. Solid State* **39**, 846 (1997)].
- ³K. Kihara and T. Sudo, *Acta Crystallogr., Sect. B: Struct. Crystallogr. Cryst. Chem.* **30**, 1088 (1974).
- ⁴M.Ya. Valakh, M.P. Lisitsa, A.V. Trilis, A. M. Yaremko, and E. Yu. Peresh, *Fiz. Tverd. Tela (St. Petersburg)* **39**, 1452 (1998) [*Phys. Solid State* **39**, 1289 (1997)].
- ⁵S.V. Melnikova, L.A. Shabanova, A.I. Zaitsev, S. A. Parshikov, O. A. Ageev, and K. S. Aleksandrov, *Ferroelectr. Lett. Sect.* **20**, 163 (1996).
- ⁶I.P. Aleksandrova, A.F. Bovina, O.A. Ageev, and A.A. Sukhovskii, *Fiz. Tverd. Tela (St. Petersburg)* **39**, 1105 (1997) [*Phys. Solid State* **39**, 991 (1997)].
- ⁷I.P. Aleksandrova, A.A. Sukhosvsky, and K.S. Aleksandrov, *Solid State Commun.* **107**, 323 (1998).
- ⁸F. Cipriani, J.-C. Castagna, M.S. Lehmann, and C. Wilkinson, *Physica B* **213**, 975 (1995).
- ⁹C.M.E. Zeyen, R. Chagnon, F. Disdier, and H. Morin, *Rev. Phys. Appl.* **19**, 789 (1984).
- ¹⁰V. Janovec, D.B. Litvin, and L. Richteroová, *Ferroelectrics* **157**, 75 (1994).
- ¹¹E.B. Loginov, *Kristallografiya* **24**, 1109 (1979) [*Sov. Phys. Crystallogr.* **24**, 637 (1979)].
- ¹²J.W. Felix, D. Mukamel, and R.M. Hornreich, *Phys. Rev. Lett.* **57**, 2180 (1986).
- ¹³G. Dolino, in *Incommensurate Phases in Dielectrics*, edited by R. Blinc and A. P. Levanyuk (North-Holland, Amsterdam, 1986), Vol. 2, p. 205.
- ¹⁴D. Durand, F. Denoyer, R. Currat, and M. Lambert, in *Incommensurate Phases in Dielectrics* (Ref. 13), Vol. 2, p. 101.
- ¹⁵S.W.H. Eijt, R. Currat, J.E. Lorenzo, P. Saint-Grégoire, S. Katanano, T. Janssen, B. Hennion, and Yu Vysochanskii, *J. Phys.: Condens. Matter* **10**, 4811 (1998).
- ¹⁶V. Janovec and L. Richteroová (unpublished).